JOURNAL OF Materials CHEMISTRY

IR laser-induced thermolysis and UV laser-induced photolysis of 1,3-diethyldisiloxane: chemical vapour deposition of nanotextured hydridoalkylsilicones†

Markéta Urbanová,[a] Zdeněk Bastl,[b] Jan Šubrt[c] and Josef Pola*[a]

[a]*Institute of Chemical Process Fundamentals, Academy of Sciences of the Czech Republic, 165 02 Prague, Czech Republic*
[b]*J. Heyrovsky Institute of Physical Chemistry, Academy of Sciences of the Czech Republic, 18223 Prague, Czech Republic*
[c]*Institute of Inorganic Chemistry, Academy of Sciences of the Czech Republic, 25068 Řež near Prague, Czech Republic*

Received 19th October 2000, Accepted 2nd April 2001
First published as an Advance Article on the web 1st May 2001

IR laser thermolysis and UV laser photolysis of gaseous 1,3-diethyldisiloxane proceed *via* different mechanisms: the former involves 1,1-H_2 and ethene elimination, whereas the latter is dominated by 1,1-H_2 and ethane elimination. The difference plays an important role in determining the composition of the solid nanotextured films deposited from the gas phase.

Introduction

Thermal decomposition of peralkylsiloxanes under conventional hot-tube conditions was examined some decades ago (*e.g.* ref. 1–6) and continued to attract further attention (*e.g.* ref. 7–9). It has been established that the major degradation mechanism is the rearrangement of the Si–O bonds. No cleavage of the weaker Si–C bond having been observed indicated that the more stable Si–O bond is broken *via* a kinetically favored path possibly involving ionic impurities or apparatus surfaces.[3]

Conversely to the hot-surface heterogeneous conditions, truly homogeneous, gas-phase IR laser-induced decomposition of hexamethyldisiloxane takes place exclusively *via* cleavage of the Si–C bonds[10,11] and some Si–O bond splitting can be only achieved under conditions close to the dielectric breakdown.[12]

The IR laser thermolysis[13–15] of gaseous methyldisiloxanes $[(CH_3)_nH_{3-n}Si]_2O$ ($n=0$–2) differs from UV laser photolytic[16,17] decomposition of these compounds: the cleavage of the Si–O bond occurs under thermolysis, but it does not take place under photolysis. Thus, the IR laser thermolysis of disiloxane ($n=0$) is dominated by molecular elimination of silane[14] and that of 1,3-dimethyldisiloxane ($n=1$)[15] and 1,1,3,3-tetramethyldisiloxane ($n=2$)[13] proceeds by the cleavage of the Si–C, Si–H and Si–O bonds. Conversely, the UV photolysis of disiloxane ($n=0$) takes place *via* cleavage of the Si–H bonds[16] and that of 1,3-dimethyldisiloxane ($n=1$) occurs *via* cleavage of the Si–C and Si–H bonds.[17]

The IR laser thermolysis and UV laser photolysis of gaseous disiloxanes[10–17] as well as pyrolytic laser-induced interaction with disiloxane aerosols[18] are convenient methods for chemical deposition of hydrogenated silicon-rich Si–O and Si–C–O films which find applications in microelectronics and are important in various fields of applied research. In these processes, the composition of the films was demonstrated to differ depending on the structure and the decomposition mechanism of the precursor.

In this paper we examine IR and UV laser-induced photolysis of gaseous 1,3-diethyldisiloxane (DEDSO) and reveal that these decompositions differ in mechanism and that they yield different solid nanotextured Si/C/H/O phases deposited from the gas phase.

Experimental

IR laser thermolytic experiments were conducted in a Pyrex tube-like (10 cm long, 3.5 cm in diameter) reactor (100 ml in volume) fitted with two KBr windows. UV laser photolytic experiments were carried out in a Pyrex reactor (140 ml in volume) consisting of two orthogonally positioned tubes (both 3.5 cm in diameter), one (10 cm long) fitted with two quartz plates and the other (13 cm long) furnished with two KBr windows. Both reactors were equipped with a port for connecting it to a vacuum manifold, a PTFE valve and a sleeve with rubber septum. A TEA CO_2 laser (Plovdiv University) operating with a frequency 1 Hz on the R(12) line of the $00^01\rightarrow10^00$ transition (970.55 cm^{-1}) was used for the thermolysis experiments; the laser beam was rectangular (0.5×1.7 cm) and was focused by a NaCl lens. An ArF (ELI 94 model) laser operating at 193 nm with a repetition frequency of 10 Hz and an incident energy of 70 mJ effective on the area of 2 cm^2 was used for the UV photolysis of DEDSO.

The progress of the DEDSO decompositions was monitored by periodically removing the reactors and placing them in the cell compartments of the FTIR (Nicolet Impact) spectrometer. The depletion of DEDSO was followed using its diagnostic absorption band at 1087 cm^{-1} and the accumulation of gaseous products was monitored by FTIR spectroscopy and by gas chromatography (a Shimadzu GC 14A chromatograph coupled with a Chromatopac C-R5A computing integrator, Porapak P column, programmed (20–150 °C) temperature, helium carrier gas). The hydrocarbon and organosilicon volatile products were identified on a Shimadzu model QP 1000 quadrupole mass spectrometer (ionizing voltage 70 eV). Hydrogen was determined on a Kratos MS 80 mass

†Electronic supplementary information (ESI) available: GC trace of volatile products from photolysis of DEDSO; XPS and Auger electron spectra of the nanotextured films. See http://www.rsc.org/suppdata/jm/b0/b008437i/

This journal is © The Royal Society of Chemistry 2001

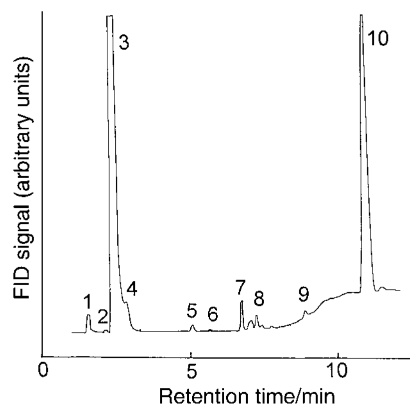

Fig. 1 Typical GC trace of volatile products from IR laser thermolysis of DEDSO (1, methane; 2, silane; 3, ethene; 4, ethane; 5, methylsilane; 6, propane; 7, disiloxane; 8, butane; 9, ethyldisiloxane; 10, DEDSO.

spectrometer using standard mixtures of hydrogen and methane. The quantitative analysis of gaseous products relied on the knowledge of the FID or TIC response factors of the authentic samples from our stock.

In order to evaluate properties of the deposited solid material by FTIR and X-ray photoelectron spectroscopy (XPS), as well as by electron microscopy, the films were produced on different substrates (KBr lumps, metal sheets) accommodated in the reactors before irradiation.

The X-ray photoelectron and Auger electron spectra were recorded in ESCA 310 (Gammadata Scienta) and ESCA 3 MkII electron spectrometers. The background pressure during the spectral measurement was in the 10^{-7} Pa range. Electron spectra were recorded using Al Kα radiation. Detailed spectral scans were taken over the Si 2p, C 1s, O 1s and Si KLL regions. The samples were measured as received and after sputtering by argon ions ($E = 5$ keV, $I = 20$ µA, $t = 5$ min). The aim of the ion sputtering was to remove the superficial layers which could be oxidized during the sample transport from the reactor to the spectrometer. The elemental surface concentrations were calculated from the photoelectron peak intensities using theoretical photoionization cross-sections.

The SEM analyses were conducted on a Philips XL30 CP Scanning Electron Microscope.

DEDSO was prepared according to the literature procedure[19] and its purity was better than 96% as checked by gas chromatography.

Results and discussion

Gaseous DEDSO (5 Torr) was decomposed by tuning the TEA CO_2 laser radiation into the absorption (δSiH_2) band centered at 969 cm^{-1} (absorptivity 0.021 $Torr^{-1}$ cm^{-1}). The ArF laser-induced photolysis of gaseous DEDSO (5 or 20 Torr) in an excess of helium gas (atmospheric pressure) was conducted by irradiating a gaseous sample at 193 nm hitting the tail of the UV absorption band with the absorptivity at 193 nm, 1.6×10^{-4} $Torr^{-1}$ cm^{-1}.

Chemistry in the gas phase

IR laser thermolysis. The laser thermolysis results in a visible luminescence after each pulse, depletion of DEDSO, the formation of gaseous products (Fig. 1) and of a solid yellowish material depositing onto the reactor surface. The relative amounts of the formed gaseous products are weakly dependent on the irradiation fluence and on the number of pulses (Table 1). The major products are ethene, hydrogen and disiloxane which are accompanied by methane, ethane, propane, butane, methylsilane and silane. The amounts of the observed hydrocarbons rule out the formation of ethyl radical being the dominant decomposition step; this species would have undergone disproportionation and recombination reactions to produce equal amounts of ethene and ethane and substantially higher amounts of butane.[20] The preponderance of ethene indicates that this product is formed by molecular expulsion and that radical steps are of low importance. However, the small amounts of the C_1–C_4 hydrocarbons are in line with a small extent of Si–C and C–C bond cleavages, recombination of the CH_3 and C_2H_5 radicals and abstraction of H from DEDSO with the CH_3 radical. The molecular (four-centre) elimination of ethene can, in principle, take place from DEDSO and ethyldisiloxane to yield disiloxane (route A), or from intermediate silylenes (route B) originating from 1,1-H_2 elimination from DEDSO (Scheme 1). The observation that disiloxane and molecular hydrogen are the main products is in keeping with the occurrence of both paths. We note that these steps were also observed in the thermolysis of structurally similar monoorganosilanes: the infrared multiphoton decomposition of monoalkylsilanes was proposed to occur *via* a four-centre elimination of silane[21,22] or 1,1-H_2 elimination,[23] and the shock-induced thermolysis of these compounds was interpreted as a blend of 1,2-H_2 and 1,1-H_2 elimination.[24,25] The minor extent of disiloxane decomposition *via* elimination and polymerization of silanone H_2Si=O is supported by the presence of silane; this reaction is a well documented process when disiloxane is exposed to TEA CO_2 laser radiation.[14,26] Ethylsilane having been not observed among the products indicates that this mode of decomposition of DEDSO and of ethyldisiloxane into ethylsilane and silanones (*e.g.* route C) is not as feasible.

Routes A and B of the DEDSO decomposition in Scheme 1 lead to different final products; the former affords perhydridosilicone, while the latter yields a silicone polymer incorporating some Si–Si bonds and ethyl and H substituents. Route B affords various silylenes which can be inferred[24,25] to undergo insertions into Si–H bonds of DEDSO and of the siloxanes produced by elimination of silanes from these products of insertion. These reactions make the total scheme of the formation of solid macromolecules rather complex.

Routes A and B are reflected in the stoichiometry of the deposit as discussed below.

UV laser photolysis. The laser photolysis results in the formation of volatile hydrocarbons and hydrogen together with a white fog observed throughout all the inside of the reactor. The fog slowly descends onto the reactor bottom and produces white solid films. No silicon-containing volatile

Table 1 Distribution of products in laser thermolysis of DEDSO

			Gaseous products (relative mol%)								
Fluence/J cm^{-2}	No. of pulses	Depletion (%)	CH_4	C_2H_4	C_2H_6	C_3H_8	C_4H_{10}	SiH_4	CH_3SiH_3	$(H_3Si)_2O$	H_2/CH_4
0.43	100	11.6	5.2	57.6	4.6	0.2	0	0.3	2.7	29.4	4.3
0.67	700	24.6	1.5	59.8	0.7	0	0.1	0.1	0.7	37.1	—
1.72	30	18.7	6.0	62.3	0.8	0.2	0	0.3	2.1	28.3	10
1.72	70	34.0	5.3	60.1	0.5	0.3	0	1.0	2.1	30.7	24

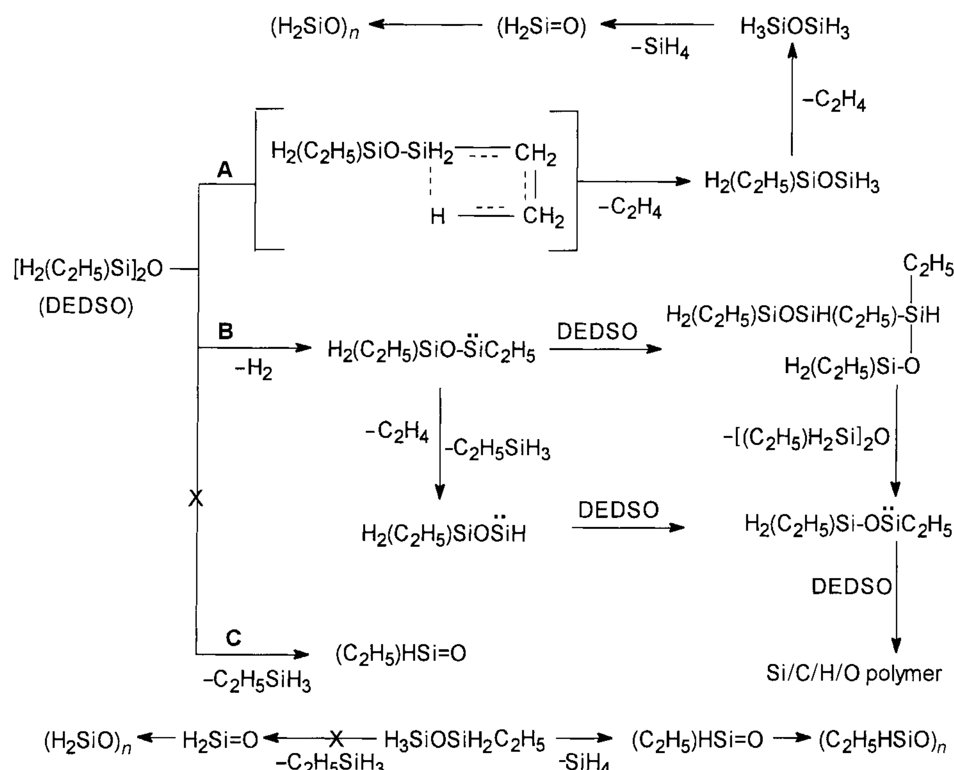

Scheme 1

products have been detected. Typical hydrocarbon product distribution as dependent on the photolysis progress (Fig. 2) reveals ethane (a major product) accompanied by smaller amounts of ethene, methane, propane and butane. The absence of Si-containing volatile products indicates that the major decomposition step is the cleavage of the Si–C and/or Si–H but not that of the Si–O bond. The energy delivered by the photons at 193 nm is equal to *ca.* 620 kJ mol^{-1} and is in excess of the energy required to split the Si–C ($\sim$370 kJ mol^{-1}), C–H ($\sim$410 kJ mol^{-1}) and Si–H ($\sim$380 kJ mol^{-1}) and even of the strong Si–O bond ($\sim$530 kJ mol^{-1}).[27] However, the Si–O bond cleavage is not a feasible photochemical step[28,29] and the expected primary photolytic processes are 1,1-H_2 and 1,1-[hydrocarbon] eliminations.[16,30,31]

The predominance of ethane among the hydrocarbons indicates that ethane originates *via* molecular extrusion. This route gets support from the known preference for combination over disproportionation of small radicals in the gas phase.[20] The low amounts of butane observed in our experiments are thus in line with an insignificant occurrence of ethyl radicals which recombine to butane and disproportionate to ethane and ethene. The observation of propane reflects the cleavage of the C–C bond and the recombination of ethyl and methyl radicals. Methane is likely formed by the abstraction of H from DEDSO. These products of radical reactions indicate that a small portion of ethane can be produced by abstraction of H by ethyl radicals from DEDSO, or by recombination of methyl radicals.

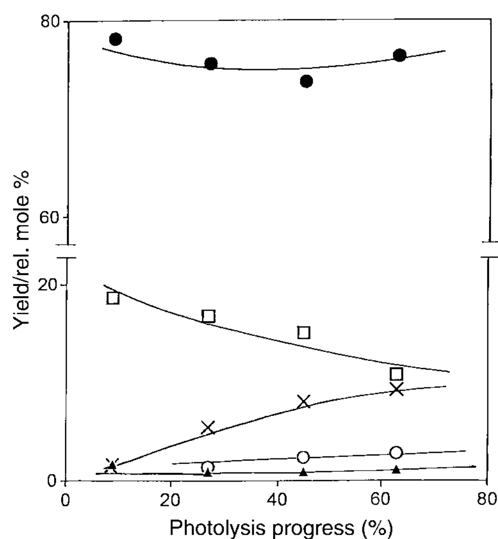

Fig. 2 Hydrocarbon product yield at different photolysis progress. (● ethane, □ ethene, × methane, ○ propane, ▲butane).

The observation of H_2 (in amounts of 1.5–1.8 times those of ethane) can be explained by 1,1-molecular elimination of H_2. Some of the plausible major and minor steps are shown in Scheme 2, where path B is that given in Scheme 1. These steps imply that, compared to DEDSO, the solid product is poorer in H and C but has the same Si : O ratio.

The formation of solid agglomerates is compatible with aggregation of silylenes taking place *via* sequences of the insertion of silylenes into the Si–H bonds of DEDSO and the siloxanes produced by elimination of silanes from these products of insertion. Thus, the total scheme of the formation of solid macromolecules is, similarly to that for the IR laser decomposition, rather complex.

Mass spectra of DEDSO and ethyldisiloxane. Comment on the fragmentation of DEDSO and ethyldisiloxane under electron impact is pertinent. The mass spectra of DEDSO [*m*/*z* (relative intensity, %) = 134 (10), 133 (41), 132 (29), 106 (13), 105 (92), 104 (20), 103 (22), 78 (16), 77 (100), 76 (14), 75 (50), 74 (11), 73 (17), 72 (7)] and of ethyldisiloxane [*m*/*z* (relative intensity, %) = 106 (11), 105 (60), 104 (10), 78 (12), 77 (100), 76 (30), 75 (48), 74 (9), 73 (17), 72 (8)] consist of signals corresponding to the loss of ethene and of 1–5 or 1–6 H atoms. Both mass spectra were obtained by GC/MS analysis. It

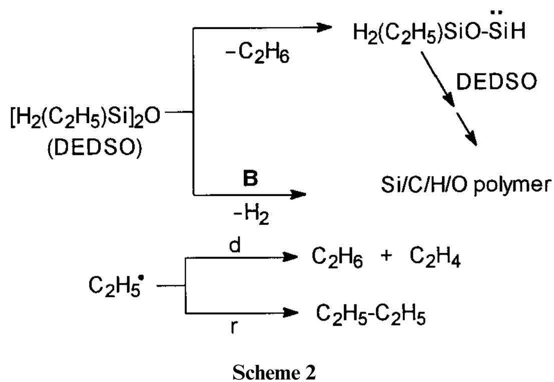

Scheme 2

is evident that the electron impact-induced fragmentation of the $(C_2H_5)H_2SiOSiH_2X$ (X = H, C_2H_5) molecules has similar features to the IR laser thermolysis of $(C_2H_5)H_2SiO$-$SiH_2(C_2H_5)$.

Deposited films

The solid films deposited from IR laser thermolysis and UV laser photolysis of DEDSO show similar IR spectral patterns (Fig. 3), consisting of bands assigned in Table 2. The absorptivity ratios $A[\nu(C\text{–}H)]:A[\nu(Si\text{–}H)]$ for the deposit from the low-fluence and high-fluence IR laser thermolysis (0.55 and 0.50, respectively) and that from the UV laser photolysis (0.57) reveal similar ratios of C–H and Si–H bonds in all the three materials. These values are in line[32] with the more than double content of the H(C) centers compared to the H(Si) centers. The absorptivity ratios $A[\nu(Si\text{–}H)]:A[\nu(Si\text{–}O)]$ with these solids are, in the given order, 0.47, 0.24 and 0.47; these values are compatible with fewer H(Si) (and also H(C)) centers in the deposit from the high-fluence IR laser thermolysis and show that reaction steps in which Si–H and C–H bonds get lost are more important in this process. The deposits from low-fluence IR laser photolysis and UV laser photolysis possess similar contents of H(Si) and H(C) centers, but their spectral pattern at 850 and 880 cm^{-1} is different and in keeping with a different Si–C–(O) framework.

XPS and Auger electron spectral analyses of the deposited films before and after sputtering by Ar ions allow us to draw inferences about the chemistry of these materials and about the relative importance of the paths proposed to take place in the gas phase.

The surface stoichiometry assessed from the intensities of the photoemission lines of the deposited films (Table 3) is discussed first. The values from the Table 3 can be compared to the stoichiometry of DEDSO $Si_1C_2O_{0.5}$ and reconciled with the observed escape of the Si, C and O elements from the formed solid product into the volatile products. The stoichiometry of the topmost (*ca.* 5 nm in depth) layers of the deposits from the low- and high-fluence laser thermolysis does not practically

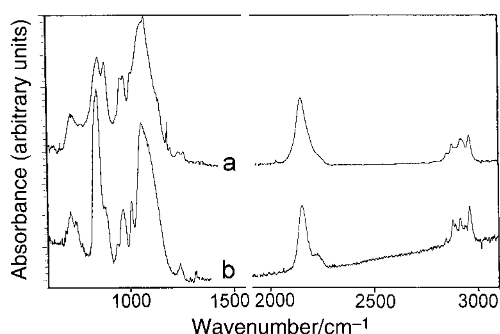

Fig. 3 FTIR spectra of the deposit from IR laser thermolysis (a) and UV laser photolysis (b) of DEDSO.

Table 2 FTIR spectra of the solid deposit from IR laser thermolysis (f = 0.67 J cm^{-2} (a) and 1.72 J cm^{-2} (b)) and UV laser photolysis (c) of DEDSO

Vibration (wavenumber/cm^{-1})	Absorptivity[a] a	b	c
ν(Si–C) + δ(Si–H) (850)	0.72	0.63	1.20
ν(Si–C) (880)	0.66	0.59	—
δSiH_2 (970)	0.60	0.54	0.36
ν(Si–O) (1080)	1.0	1.0	1.0
ν(Si–H) (2150)	0.47	0.24	0.47
ν(C–H) (2980)	0.15	0.07	0.17
ν(C–H) (2920)	0.17	0.11	0.18
ν(C–H) (2960)	0.26	0.12	0.27

[a]Normalized to that of the ν(Si–O) band.

differ and suggests that proposed route B is a significant pathway, since the exclusive operation of route A would have afforded an unobserved Si–O material. The determined stoichiometry of the topmost layers of the deposits reveals that the material from the UV laser photolysis possesses more carbon than the deposits from the IR laser thermolysis. This is in accordance with the occurrence of carbon-richer polymerizable transients in the UV laser-induced process. The amount of oxygen in all the deposits being higher than 0.5 of that of silicon indicates that the superficial layers are prone to oxidation and that they uptake oxygen from air when the deposit is transferred for the XPS analysis.

More detailed insight into the chemistry of these materials is provided by the Si 2p core level spectra as well as the more resolved Si $KL_{23}L_{23}$ Auger electron spectra that reveal that these films are composed of different components. Three chemical states of Si are observed in the electron spectra of samples from the IR laser thermolysis, while only one state has been identified in samples from the UV laser photolysis (Table 4).

The films deposited by the IR laser thermolysis are composed of small amounts of elemental silicon (designated as $Si^{(1)}$), a silicon in a polymer whose chemical environment is similar to that in oxosilanes (designated as $Si^{(2)}$), and of an $Si^{(3)}$ silicon which can be interpreted as a product of interaction of the $Si^{(2)}$ state with atmospheric oxygen and/or moisture. The $Si^{(3)}$ state predominates in the as received samples, but upon ion sputtering its population decreases and those of the $Si^{(1)}$ and $Si^{(2)}$ states increase. The above assignments are based on comparison of the measured spectral data with the published ones.[33]

The films produced by the UV laser photolysis contain only one chemical state of Si which is not identical to any of the states found in the deposits produced by the IR laser thermolysis. The measured binding energy of Si 2p electrons as well as the kinetic energy of Si KLL electrons fall within the range of values expected for Si/C/O/H polymers.[33] The ion sputtering of this material leads to broadening of the spectra and shifting of the Auger peak by 2.4 eV towards higher kinetic energies. This shift is much higher than the shift of the Si 2p line, 0.3 eV and can be interpreted as being caused by increased extraatomic relaxation due to modification of the polymer structure by argon ions. We did not observe such large shifts of

Table 3 Stoichiometry[a] of the deposits determined by XPS analysis

Deposition method	Before[b]	After[c]
Laser thermolysis, f = 0.67 J cm^{-2}	$Si_{1.0}C_{0.8}O_{1.2}$	$Si_{1.0}C_{0.6}O_{0.9}$
Laser thermolysis f = 1.72 J cm^{-2}	$Si_{1.0}C_{1.0}O_{1.5}$	$Si_{1.0}C_{0.8}O_{1.1}$
UV laser photolysis	$Si_{1.0}C_{1.8}O_{0.9}$	$Si_{1.0}C_{1.1}O_{0.8}$

[a]±10%. [b]Sample as received. [c]Sample after sputtering by argon ions.

Table 4 Si 2p core level binding energies and populations of individual chemical states of Si in the deposits

	Si 2p binding energy/eV [population (%)]					
	Deposit from laser thermolysis, $f = 0.67$ J cm^{-2}		Deposit from laser thermolysis, $f = 1.72$ J cm^{-2}		Deposit from UV laser photolysis	
Silicon environment	Before[a]	After[b]	Before[a]	After[b]	Before[a]	After[b]
$Si^{(1)}$	99.5 [9]	99.5 [15]	99.9 [8]	99.8 [56]	—	—
$Si^{(2)}$	101.0 [12]	101.1 [57]	101.0 [11]	101.7 [30]	—	—
$Si^{(3)}$	102.6 [79]	103.0 [28]	102.8 [81]	102.8 [14]	—	—
Si	—	—	—	—	102.0 [100]	102.3 [100]

[a]Sample as received. [b]Sample after sputtering by argon ions.

Auger spectra with ion sputtering for films produced by IR laser thermolysis.

In an attempt to explain the presence of the $Si^{(1)}$, $Si^{(2)}$ and $Si^{(3)}$ forms in the deposit from the IR laser-induced thermolysis, and the absence of these forms in the deposit from the UV laser photolysis, we assume that the elemental silicon is mostly formed from the detected silane. Indeed, the infrared multiphoton decomposition of silane into elemental silicon is well documented in the literature.[34–36] The population of the elemental Si in the deposit obtained at the low-fluence irradiation is lower than that obtained at the high-fluence irradiation; this indicates that the higher fluences of radiation facilitate silane decomposition. Both the $Si^{(2)}$ form produced by IR laser photolysis and the Si form produced by UV laser photolysis are silicones, but their differing Si 2p binding energies result from different structures. The formation of the $Si^{(2)}$ type is caused by reactions of silanone, $H_2Si{=}O$ which is formed by the IR laser-induced decomposition of disiloxane.[26] The silanone can isomerize into hydroxysilylene (HO)HSi:[37,38] which can decompose into elemental silicon and water, or react with molecular hydrogen to yield silanol. These steps were shown to occur in IR laser-induced thermolysis of disiloxane,[26] but their occurrence in the UV laser photolysis is not substantiated. The formation of the $Si^{(3)}$ form upon exposure of the $Si^{(2)}$ form to air obviously relates to some presence of unsaturated silicon centers which are not appreciably produced by the UV photolysis.

Scanning electron microscopy analysis reveals that all the deposits, regardless of their formation under different irradiation conditions, consist of nanotextured agglomerates which are bonded together (Fig. 4). This feature is in keeping with the agglomeration occurring in the gas phase and may indicate that once deposited, the agglomerates increase their size also after having been deposited on the substrate.

All the deposits are insoluble in organic solvents (ethanol, diethyl ether, chloroform, hexane and toluene), which indicates their high molecular weight and/or cross-linked structure.

Conclusion

The TEA CO_2 laser thermolysis of DEDSO is initiated by elimination of H_2 and ethene, whereas ArF laser photolysis begins as elimination of H_2 and ethane. Both processes proceed as a multitude of subsequent reactions and differ in the final products. The IR laser-induced thermolysis of DEDSO yields hydrogen, hydrocarbons and Si- and O-containing volatile compounds and affords chemical vapour deposition of solid hydridoalkylsilicone films containing elemental silicon. The UV laser-induced photolysis of DEDSO results in the

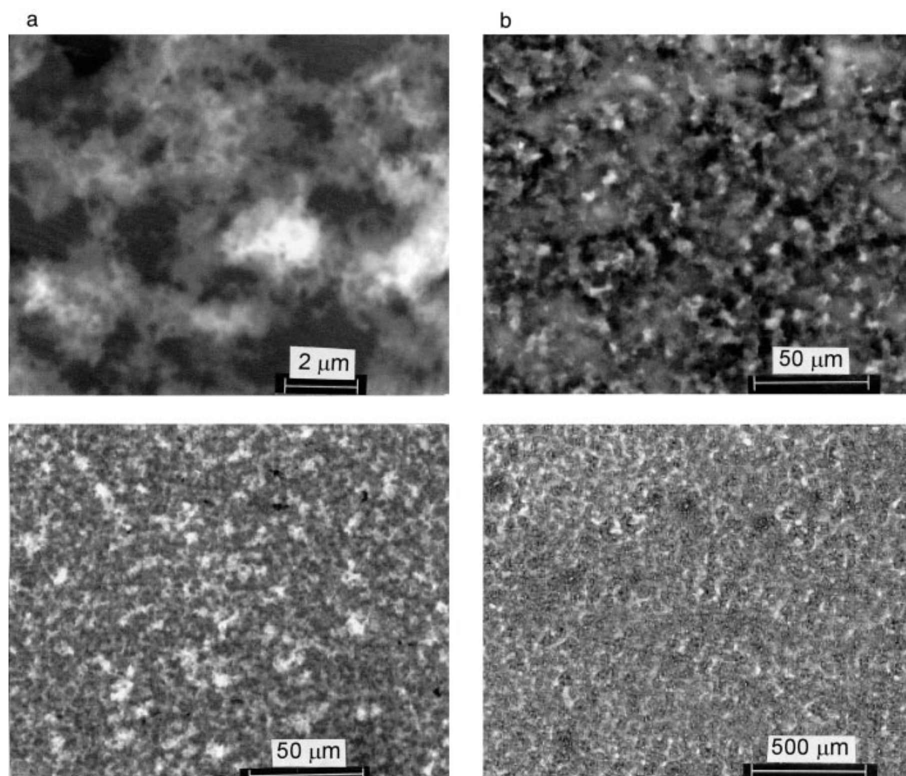

Fig. 4 SEM of the deposit obtained by IR laser thermolysis (a) and UV laser photolysis (b) of DEDSO.

formation of hydrogen and hydrocarbons and affords chemical vapour deposition of solid hydridoalkylsilicone films.

Acknowledgements

The work was supported by GAAVCR of the Czech Republic (grant no. A4072806). The authors thank Mr J. Kupčík for MS determination of hydrogen.

References

1 N. Patnode and D. F. Wilcock, *J. Am. Chem. Soc.*, 1946, **68**, 358.
2 C. W. Lewis, *J. Polym. Sci.*, 1958, **33**, 153.
3 T. H. Thomas and T. C. Kendrick, *J. Polym. Sci., Polym. Phys. Ed.*, 1969, **7**, 537.
4 T. H. Thomas and T. C. Kendrick, *J. Polym. Sci., Polym. Phys. Ed.*, 1970, **8**, 1823.
5 N. Grassie and I. G. MacFarlane, *Eur. Polym. J.*, 1978, **14**, 875.
6 J. M. Nielsen, *J. Appl. Polym. Sci., Appl. Polym. Symp.*, 1979, **35**, 223.
7 D. A. White, S. M. Oleff and J. R. Fox, *Adv. Ceram. Mater.*, 1987, **2**, 53.
8 R. B. Taylor and G. A. Zank, *Polym. Prepr. (Am. Chem. Soc., Div. Polym. Chem.)*, 1991, **32**, 586.
9 A. M. Wilson, G. Zank, K. Euguchi, W. Xing, B. Yates and J. R. Dahn, *Chem. Mater.*, 1997, **9**, 1601.
10 W. F. Manders and J. M. Bellama, *J. Polym. Sci., Polym. Chem. Ed.*, 1985, **23**, 351.
11 J. Pola, R. Alexandrescu, J. Morjan and D. Sorescu, *J. Anal. Appl. Pyrolysis*, 1990, **18**, 71.
12 J. Kupčík, Z. Bastl, J. Šubrt, J. Pola, V. C. Papadimitriou, A. V. Prosmitis and P. Papagiannakopoulos, *J. Anal. Appl. Pyrolysis*, 2001, **57**, 109.
13 J. Pola, D. Pokorná, Z. Bastl and J. Šubrt, *J. Anal. Appl. Pyrolysis*, 1996, **38**, 153.
14 J. Pola, M. Urbanová, V. Dřínek, J. Šubrt and H. Beckers, *Appl. Organomet. Chem.*, 1999, **13**, 655.
15 J. Pola, M. Urbanová, Z. Bastl, J. Šubrt and P. Papagiannakopoulos, *J. Mater. Chem.*, 2000, **10**, 1415.
16 J. Pola, M. Urbanová, Z. Bastl, J. Šubrt and H. Beckers, *J. Mater. Chem.*, 1999, **9**, 2429.
17 J. Pola, A. Ouchi, Z. Bastl, J. Šubrt, M. Sakuragi, A. Galíkova and A. Galík, *Chem. Vap. Deposition*, 2001, **7**, 19.
18 Y. El Kortobi, J.-B. d'Espinose de la Caillerie, A.-P. Legrand, X. Armand, N. Herlin and M. Cauchetier, *Chem. Mater.*, 1997, **9**, 632.
19 P. Bissinger, M. Paul, J. Riede and H. Schmidbaur, *Chem. Ber.*, 1993, **126**, 2579.
20 M. J. Gibian and R. C. Corley, *Chem. Rev.*, 1973, **73**, 441.
21 J. S. Francisco, S. A. Joyce, J. I. Steinfeld and F. Walsh, *J. Phys. Chem.*, 1984, **88**, 3098.
22 J. W. Thoman and J. I. Steinfeld, *Chem. Phys. Lett.*, 1986, **124**, 35.
23 D. M. Rayner, R. P. Steer, P. A. Hackett, C. L. Wilson and P. John, *Chem. Phys. Lett.*, 1986, **123**, 449.
24 S. F. Rickborn, M. A. Ring and H. E. O'Neal, *Int. J. Chem. Kinet.*, 1984, **16**, 1371.
25 M. A. Ring, H. E. O'Neal, S. F. Rickborn and B. A. Sawrey, *Organometallics*, 1983, **2**, 1891.
26 J. Pola, Z. Bastl, M. Urbanová, J. Šubrt and H. Beckers, *Appl. Organomet. Chem.*, 2000, **14**, 453.
27 R. Walsh, in *The Chemistry of Organic Silicon Compounds*, eds. S. Patai and Z. Rappoport, Wiley, Chichester, 1989, ch. 5
28 J. C. Dalton, in *Organic Photochemistry*, ed. A. Padwa, Marcel Dekker, New York, 1985, Vol. 7, ch. 3
29 A. Ouchi, A. Koga, Z. Bastl and J. Pola, *Appl. Organomet. Chem.*, 1999, **13**, 643.
30 G. Inoue and M. Suzuki, *Chem. Phys. Lett.*, 1984, **105**, 641.
31 S. E. Rickborn, M. A. Ring, H. E. O'Neal and D. Coffey, *Int. J. Chem. Kinet.*, 1984, **16**, 289.
32 H. C. Low and P. John, *J. Organomet. Chem.*, 1980, **201**, 363 and refs. therein.
33 *NIST X-Ray Photoelectron Spectroscopy Database*, Ver. 2.0, NIST, Gaithersburg, 1997
34 A. N. Oraevski, A. V. Pankratov, A. N. Skachkov and V. M. Shabarshin, *Khim. Vys. Energ.*, 1978, **12**, 59.
35 T. F. Deutsch, *J. Chem. Phys.*, 1979, **70**, 1187.
36 P. A. Longway and F. W. Lampe, *J. Am. Chem. Soc.*, 1981, **103**, 6813.
37 C. L. Darling and H. B. Schlegel, *J. Phys. Chem.*, 1993, **97**, 8207.
38 B. Ma, N. Allinger and H. F. Schaefer, *J. Chem. Phys.*, 1996, **105**, 5731.